

Supplementary Information

A combined experimental and theoretical studies on a series of mononuclear Ln^{III} single-molecule magnets: a dramatic influence of remote substitution on magnetic dynamics in Dy analogues

Kuheli Pramanik,^{a,b} Zvonko Jagličić,^c Radovan Herchel,^d Paula Brandão,^e Narayan Ch. Jana,^b and Anangamohan Panja^{*a,b}

^a Department of Chemistry, Gokhale Memorial Girls' College, 1/1 Harish Mukherjee Road, Kolkata-700020, India. E-mail: ampanja@yahoo.co.in

^b Department of Chemistry, Panskura Banamali College, Panskura RS, WB 721152, India

^c Institute of Mathematics, Physics and Mechanics & Faculty of Civil and Geodetic Engineering, University of Ljubljana, Jadranska 19, 1000 Ljubljana, Slovenia

^d Department of Inorganic Chemistry, Faculty of Science, Palacký University, 17. listopadu 12, 77146 Olomouc, Czech Republic

^e Department of Chemistry, CICECO-Aveiro Institute of Materials, University of Aveiro, 3810-193 Aveiro, Portugal

* Corresponding author e-mail: ampanja@yahoo.co.in

Table of Contents

Table S1: Crystallographic parameters of the complexes.....	5
Table S2. SHAPE analysis of the Ln ^{III} ion in complexes 1Dy–6Gd.....	6
Table S3. Relaxation fitting parameters from the least-square fitting of the Cole-Cole plots of 1 by the single-component generalized Debye model at zero and 1000 Oe dc fields.....	6
Table S4. Relaxation fitting parameters from the least-square fitting of the Cole-Cole plots of 6 by the single-component generalized Debye model at zero and 1000 Oe dc fields.....	7
Table S5. Relaxation fitting parameters from the least-square fitting of the Cole-Cole plots of 2 by the single-component generalized Debye model at 1000 Oe dc fields.....	9
Table S6. Relaxation fitting parameters from the least-square fitting of the Cole-Cole plots of 4 by the single-component generalized Debye model at 1000 Oe dc fields.....	10
Table S7. Relaxation fitting parameters from the least-square fitting of the Cole-Cole plots of 5 by the single-component generalized Debye model at 1000 Oe dc fields.....	11
Table S8. The splitting of the lowest multiplets for Ln ^{III} ions in 1–6 compounds calculated by CASSCF method	12
Table S9. The g-factors for the effective spin 1/2 calculated by CASSCF for lowest Kramers (pseudo)doublets of 1–6	13
Table S10. Comparison of U _{eff} value of this work with the other reported mononuclear Yb ^{III} SMMs. ^a	14
Table S11. Comparison of U _{eff} value of this work with the other reported Dy ^{III} SMMs with N-salicylideneaniline type ligands in the zwitterionic form. ^a	15
Fig. S1. ¹ H NMR spectrum of ligand LH in CDCl ₃ at r.t.	16
Fig. S2. ¹³ C NMR of ligand LH in CDCl ₃ at r.t.....	16
Fig. S3. IR spectra of the ligands and complexes 1–6	17
Fig. S5. Crystal structures of complexes 1–5 with ellipsoid plots (probability level 30 %).....	19
Fig. S6: Crystal packing of complex 1 focusing on the π···π stacking interaction	19
Fig. S7. Isothermal magnetization curves for complexes 1–6 at 2 K.	20
Fig. S8. Frequency dependent out-of-phase ac susceptibility plots of 1 in zero dc field (left) and 1 kOe dc field (right).	20
Fig. S9. Frequency dependent in-phase and out-of-phase ac susceptibility plots of 6 at indicated dc field.	21
Fig. S10. Cole-Cole plot for 1 at zero dc field (left) and 1 kOe dc field (right)	22
Fig. S11. Cole-Cole plot for 6 at zero dc field.....	22
Fig. S12. Out-of-phase ac susceptibility as a function of dc magnetic field (left) and frequency (right) for 1 measured at 2 K.....	23
Fig. S13. Out-of-phase ac susceptibility as a function of dc magnetic field (left) and frequency (right) for 2 measured at 2 K.....	23

Fig. S14. Out-of-phase ac susceptibility as a function of dc magnetic field (left) and frequency (right) for 3 measured at 2 K.....	24
Fig. S15. Out-of-phase ac susceptibility as a function of dc magnetic field (left) and frequency (right) for 4 measured at 1.9 K.....	24
Fig. S16. Out-of-phase ac susceptibility as a function of dc magnetic field (left) and frequency (right) for 5 measured at 2 K.....	25
Fig. S17. Out-of-phase ac susceptibility as a function of dc magnetic field (left) and frequency (right) for 6 measured at 2 K.....	25
Fig. S18. The plot of magnetisation relaxation time in the form of $\ln(\tau)$ vs. T^{-1} (left) and $\ln(\tau)$ vs. $\ln(T)$ (right); solid lines in the plots denoting the best fit considering only two Orbach like relaxations (left) and the linear fit (right); insets showing the best fit parameters.....	26
Fig. S19. Frequency dependent in-phase and out-of-phase ac susceptibility plots of 2 at indicated dc field.....	26
Fig. S20. Frequency dependent in-phase and out-of-phase ac susceptibility plots of 4 at indicated dc field.....	27
Fig. S22 The molecular structure of complex 1 derived from the experimental X-ray geometry used for CASSCF calculations done in ORCA overlaid with principal axis of g-tensor of the first Kramers doublet (x/y/z-axes colored as red/green/blue arrows).....	28
Fig. S23 The molecular structure of complex 6 derived from the experimental X-ray geometry used for CASSCF calculations done in ORCA overlaid with principal axis of g-tensor of the first Kramers doublet (x/y/z-axes colored as red/green/blue arrows).....	29
Fig. S24 The molecular structure of complex 4 derived from the experimental X-ray geometry used for CASSCF calculations done in ORCA overlaid with principal axis of g-tensor of the first Kramers doublet (x/y/z-axes colored as red/green/blue arrows).....	30
Fig. S25 The molecular structure of complex 5 derived from the experimental X-ray geometry used for CASSCF calculations done in ORCA overlaid with principal axis of g-tensor of the first Kramers doublet (x/y/z-axes colored as red/green/blue arrows).....	31
Fig. S26 The molecular structure of complex 2 derived from the experimental X-ray geometry used for CASSCF calculations done in ORCA overlaid with principal axis of g-tensor of the first Kramers doublet (x/y/z-axes colored as red/green/blue arrows).....	32
Fig. S27 The molecular structure of complex 3 derived from the experimental X-ray geometry used for CASSCF calculations done in ORCA overlaid with principal axis of g-tensor of the first Kramers doublet (x/y/z-axes colored as red/green/blue arrows).....	33
Fig. S28 The analysis of magnetic properties of 1 by POLY_ANISO module. Top: The molecular structure of supramolecular dimer of 1 derived from the experimental X-ray geometry and calculated magnetic data for such dimer using POLY_ANISO program based on respective CASSCF calculations without dipolar interaction (black line) / with dipolar interaction (red line). Bottom: The fit of experimental magnetic data utilizing CASSCF calculations, POLY_ANISO program and homemade routine with the exchange parameter $J_{Dy-Dy} = -0.180 \text{ cm}^{-1}$, scaling factor for calculated data: 0.973.....	34

Fig. S29 The analysis of magnetic properties of 6 by POLY_ANISO module. <i>Top:</i> The molecular structure of supramolecular dimer of 6 derived from the experimental X-ray geometry and calculated magnetic data for such dimer using POLY_ANISO program based on respective CASSCF calculations without dipolar interaction (black line) / with dipolar interaction (red line). <i>Bottom:</i> The fit of experimental magnetic data utilizing CASSCF calculations, POLY_ANISO program and homemade routine with the exchange parameter $J_{\text{Dy-Dy}} = -0.0024 \text{ cm}^{-1}$, scaling factor for calculated data: 0.994.	35
References	36

Table S1: Crystallographic parameters of the complexes.

	1	2	3	4	5	6
Empirical formula	C ₃₀ H ₃₂ N ₅ O ₁₆ Dy	C ₃₀ H ₃₂ N ₅ O ₁₆ Tb	C ₃₀ H ₃₂ N ₅ O ₁₆ Ho	C ₃₀ H ₃₂ N ₅ O ₁₆ Er	C ₃₀ H ₃₂ N ₅ O ₁₆ Yb	C ₃₂ H ₃₆ N ₅ O ₁₆ Dy
Formula weight	881.10	877.52	883.53	885.86	891.64	909.16
Temperature/K	150(2)	150(2)	150(2)	150(2)	150(2)	150(2)
Crystal system	triclinic	triclinic	triclinic	triclinic	triclinic	triclinic
Space group	P $\bar{1}$	P $\bar{1}$	P $\bar{1}$	P $\bar{1}$	P $\bar{1}$	P $\bar{1}$
a/ \AA	10.2927(12)	10.3031(10)	10.3010(5)	10.3019(13)	10.3120(5)	10.232(2)
b/ \AA	11.8324(14)	11.8232(12)	11.8039(6)	11.8026(16)	11.7797(6)	12.552(2)
c/ \AA	14.4365(18)	14.4659(13)	14.4529(7)	14.448(2)	14.4411(8)	14.195(3)
$\alpha/^\circ$	89.489(7)	89.493(5)	89.278(2)	89.120(4)	89.020(3)	89.362(5)
$\beta/^\circ$	77.986(7)	78.117(5)	78.052(2)	78.070(4)	78.107(2)	78.082(7)
$\gamma/^\circ$	76.638(7)	76.854(5)	76.709(2)	76.718(4)	76.588(2)	78.575(6)
Volume/ \AA^3	1671.7(4)	1677.9(3)	1672.10(14)	1671.8(4)	1668.86(15)	1747.7(6)
Z	2	2	2	2	2	2
$\rho_{\text{calc}}/\text{g/cm}^3$	1.750	1.737	1.755	1.760	1.774	1.728
μ/mm^{-1}	2.319	2.191	2.450	2.594	2.886	2.221
F(000)	882.0	880.0	884.0	886.0	890.0	914.0
2 Θ range for data collection/ $^\circ$	2.886 to 54.482	2.88 to 55.92	4.488 to 61.092	2.882 to 52.904	2.884 to 54.524	2.934 to 51.482
Reflections collected	22017	33155	81792	26596	24573	18918
Independent reflections	7453 [$R_{\text{int}} = 0.0449$, $R_{\text{sigma}} = 0.0547$]	8027 [$R_{\text{int}} = 0.0568$, $R_{\text{sigma}} = 0.0522$]	10251 [$R_{\text{int}} = 0.0371$, $R_{\text{sigma}} = 0.0243$]	6854 [$R_{\text{int}} = 0.0688$, $R_{\text{sigma}} = 0.0752$]	7430 [$R_{\text{int}} = 0.0390$, $R_{\text{sigma}} = 0.0428$]	6551 [$R_{\text{int}} = 0.0604$, $R_{\text{sigma}} = 0.0753$]
Data/restraints/parameters	7453/0/497	8027/0/497	10251/0/497	6854/0/497	7430/0/497	6551/3/526
Goodness-of-fit on F^2	1.024	1.055	1.039	0.998	1.056	1.044
Final R indexes	$R_1 = 0.0314$, [I $>= 2\sigma$ (I)] $wR_2 = 0.0578$	$R_1 = 0.0332$, $wR_2 = 0.0724$	$R_1 = 0.0189$, $wR_2 = 0.0391$	$R_1 = 0.0384$, $wR_2 = 0.0714$	$R_1 = 0.0270$, $wR_2 = 0.0569$	$R_1 = 0.0421$, $wR_2 = 0.0880$
Final R indexes [all data]	$R_1 = 0.0422$, $wR_2 = 0.0612$	$R_1 = 0.0451$, $wR_2 = 0.0783$	$R_1 = 0.0252$, $wR_2 = 0.0406$	$R_1 = 0.0525$, $wR_2 = 0.0768$	$R_1 = 0.0322$, $wR_2 = 0.0589$	$R_1 = 0.0555$, $wR_2 = 0.0936$
Largest diff. peak/hole / e \AA^{-3}	0.90/-1.02	1.44/-1.40	0.63/-0.66	1.30/-0.97	1.15/-0.46	0.93/-1.15

Table S2. SHAPE analysis of the LnIII ion in complexes 1Dy–6Gd.

Label	Shape	Symmetry	1_{Gd}	2_{Dy}	3_{Gd}	4_{Dy}	5_{GD}	6_{Dy}
EP-9	Enneagon	<i>D</i> _{9h}	35.534	35.430	35.522	35.386	35.340	35.450
OPY-9	Octagonal pyramid	<i>C</i> _{8v}	21.385	21.325	21.453	21.502	21.582	21.500
HBPY-9	Heptagonal bipyramid	<i>D</i> _{7h}	16.872	16.821	16.998	17.070	17.310	16.741
JTC-9	Johnson triangular cupola J3	<i>C</i> _{3v}	16.891	16.915	16.805	16.741	16.563	16.524
JCCU-9	Capped cube J8	<i>C</i> _{4v}	9.381	9.365	9.317	9.313	9.359	9.656
CCU-9	Spherical-relaxed capped cube	<i>C</i> _{4v}	7.964	7.940	7.916	7.924	8.024	8.265
JCSAPR-9	Capped square antiprism J10	<i>C</i> _{4v}	2.829	2.866	2.779	2.720	2.675	3.026
CSAPR-9	Spherical capped square antiprism	<i>C</i> _{4v}	1.826	1.862	1.787	1.733	1.728	2.045
JTCTPR-9	Tricapped trigonal prism J51	<i>D</i> _{3h}	3.388	3.434	3.305	3.222	3.107	3.473
TCTPR-9	Spherical tricapped trigonal prism	<i>D</i> _{3h}	1.611	1.640	1.582	1.540	1.482	1.674
JTDIC-9	Tridiminished icosahedron J63	<i>C</i> _{3v}	12.333	12.253	12.382	12.492	12.355	12.463
HH-9	Hula-hoop	<i>C</i> _{2v}	11.122	11.114	11.036	11.007	11.068	10.707
MFF-9	Muffin	<i>C</i> _s	2.401	2.434	2.384	2.323	2.301	2.288

Table S3. Relaxation fitting parameters from the least-square fitting of the Cole-Cole plots of 1 by the single-component generalized Debye model at zero and 1000 Oe dc fields.

<i>T</i> (K)	χ_s (emu/mol)	$\Delta\chi$ (emu/mol)	τ (s)	α
At zero dc field				
1.9	1.2765	1.2912	3.36058E-5	0.50772
2.0	1.34491	1.17066	3.23024E-5	0.49355
2.1	1.39472	1.08152	3.02308E-5	0.48958
2.3	1.40412	1.00986	2.27367E-5	0.49254
2.4	1.37441	1.00936	1.76728E-5	0.50116
2.5	1.30489	1.04974	1.26607E-5	0.51156
2.6	1.31385	1.0114	1.18287E-5	0.50683
2.7	1.23707	1.06055	8.35194E-6	0.51712
2.8	1.32842	0.94162	9.49473E-6	0.51581
2.9	1.33295	0.90937	8.92779E-6	0.51627
3.0	1.10923	1.10662	4.37123E-6	0.53084
3.1	1.24992	0.93833	6.06339E-6	0.52176
3.2	1.24895	0.91243	5.57239E-6	0.52585
3.3	1.15662	0.97765	3.86798E-6	0.53435
At 1000 Oe dc field				
2.48	1.87532	0.51241	0.02755	0.3767
2.67	1.87838	0.45083	0.02054	0.3294

2.87	1.85946	0.40558	0.01557	0.29451
3.06	1.83165	0.37184	0.0117	0.26242
3.25	1.77594	0.37842	0.00767	0.30287
3.45	1.74646	0.34854	0.00582	0.26455
3.64	1.70957	0.32687	0.00429	0.23461
3.83	1.67147	0.30906	0.00312	0.21055
4.03	1.60975	0.32017	0.00193	0.24595
4.22	1.55222	0.32798	0.00124	0.26535
4.41	1.49067	0.34433	7.81E-04	0.29603
4.6	1.43633	0.35086	5.07E-04	0.30775
4.8	1.40129	0.33997	3.75E-04	0.29674
5	1.34901	0.3462	2.44E-04	0.30521
5.5	1.2473	0.34194	1.05E-04	0.32655
6	1.14808	0.3463	4.44E-05	0.36909
6.5	1.10299	0.30916	2.77E-05	0.39751
7	1.04637	0.29105	1.58E-05	0.43792
7.5	0.96222	0.30746	7.01E-06	0.4815

Table S4. Relaxation fitting parameters from the least-square fitting of the Cole-Cole plots of 6 by the single-component generalized Debye model at zero and 1000 Oe dc fields.

T (K)	χ_s (emu/mol)	$\Delta\chi$ (emu/mol)	τ (s)	α
At zero dc field				
2	0.55707	5.40728	9.72E-04	0.13261
3	0.40594	3.60678	8.45E-04	0.12275
4	0.3058	2.7042	7.19E-04	0.14111
5	0.25359	2.1594	6.17E-04	0.14402
6	0.22139	1.79701	5.46E-04	0.14637
7	0.19301	1.54043	4.80E-04	0.14398
8	0.17006	1.35336	4.29E-04	0.1451
9	0.15992	1.19125	3.82E-04	0.13094
10	0.15399	1.06466	3.42E-04	0.11373
11	0.14875	0.96763	3.03E-04	0.09513
12	0.12957	0.87889	2.50E-04	0.08003
13	0.12344	0.8173	2.12E-04	0.06197
14	0.11144	0.76341	1.74E-04	0.04442
15	0.0813	0.73604	1.32E-04	0.04176
16	0.10111	0.66205	1.09E-04	0.00627
17	0.08076	0.64222	8.10E-05	0.01017
18	0.03004	0.65334	5.50E-05	0.0215

At 1000 Oe dc field				
4.5	0.19201	2.94582	9.73E-01	0.25208
5	0.19025	2.39121	4.30E-01	0.18598
5.5	0.17978	2.09776	2.26E-01	0.14655
6	0.1704	1.88585	1.29E-01	0.11539
6.5	0.16181	1.71302	8.00E-02	0.0974
7	0.14968	1.58872	5.02E-02	0.08581
7.5	0.14091	1.48538	3.30E-02	0.08325
8	0.13638	1.38495	2.20E-02	0.05784
8.5	0.12852	1.31006	1.51E-02	0.05766
9	0.12022	1.23324	1.06E-02	0.05549
9.5	0.11423	1.17551	7.53E-03	0.05318
10	0.11075	1.10472	5.39E-03	0.04325
10.5	0.10419	1.05137	3.94E-03	0.04155
11	0.09944	1.01086	2.95E-03	0.04295
11.5	0.09366	0.97521	2.24E-03	0.04683
12	0.09098	0.91775	1.62E-03	0.03647
12.5	0.08778	0.88173	1.25E-03	0.03488
13	0.08523	0.85006	9.74E-04	0.03323
13.5	0.08273	0.81985	7.61E-04	0.03359
14	0.07801	0.79149	5.95E-04	0.03219
14.5	0.07263	0.76724	4.66E-04	0.03322
15	0.07377	0.73838	3.72E-04	0.02785
15.5	0.06898	0.71946	2.94E-04	0.02896
16	0.06505	0.69885	2.34E-04	0.02896
16.5	0.06659	0.67435	1.88E-04	0.02497
17	0.05852	0.66112	1.50E-04	0.02613
17.5	0.05998	0.63789	1.22E-04	0.01504
18	0.05784	0.62257	9.81E-05	0.02023
18.5	0.03747	0.62583	7.62E-05	0.0273
19	0.04774	0.59796	6.34E-05	0.02296
19.5	0.04154	0.58691	5.13E-05	0.0215
20	0.03426	0.57943	4.19E-05	0.02011
21	0.03723	0.54799	2.84E-05	0.02124
22	0.04208	0.51715	1.97E-05	0.02293

Table S5. Relaxation fitting parameters from the least-square fitting of the Cole-Cole plots of 2 by the single-component generalized Debye model at 1000 Oe dc fields.

T (K)	χ_s (emu/mol)	$\Delta\chi$ (emu/mol)	τ (s)	α
At 1 kOe dc field				
2.29	0.80486	2.8741	3.78E-04	0.37463
2.48	0.7892	2.68681	3.32E-04	0.33877
2.67	0.7762	2.5351	3.01E-04	0.30619
2.87	0.76179	2.40255	2.77E-04	0.27907
3.06	0.72814	2.3143	2.54E-04	0.26625
3.25	0.72719	2.18093	2.37E-04	0.24154
3.45	0.715	2.06778	2.19E-04	0.22258
3.64	0.68092	1.99489	2.01E-04	0.21793
3.83	0.68159	1.87794	1.88E-04	0.20118
4.03	0.68226	1.76665	1.76E-04	0.18343
4.22	0.66858	1.68086	1.63E-04	0.17294
4.41	0.65607	1.60462	1.51E-04	0.1663
4.61	0.64683	1.52737	1.40E-04	0.15661
4.8	0.63788	1.45587	1.30E-04	0.14872
5	0.62454	1.39054	1.19E-04	0.14048
5.5	0.59796	1.24289	9.55E-05	0.12961
6	0.58552	1.10735	7.93E-05	0.12115
6.5	0.65536	0.92405	7.99E-05	0.0957
7	0.63557	0.83623	7.05E-05	0.09089
7.5	0.62614	0.7508	6.45E-05	0.07964
8	0.5939	0.69873	5.58E-05	0.07133
8.5	0.55413	0.66464	4.60E-05	0.06482
9	0.49993	0.65331	3.44E-05	0.06494
9.5	0.40465	0.68789	2.24E-05	0.06781

Table S6. Relaxation fitting parameters from the least-square fitting of the Cole-Cole plots of 4 by the single-component generalized Debye model at 1000 Oe dc fields.

T (K)	χ_s (emu/mol)	$\Delta\chi$ (emu/mol)	τ (s)	α
At 1 kOe dc field				
1.9	0.31848	2.68397	2.32E-03	0.25636
2.1	0.28659	2.3756	1.53E-03	0.26767
2.29	0.26752	2.21421	1.11E-03	0.27633
2.48	0.26272	2.0556	8.03E-04	0.27485
2.67	0.2704	1.90743	6.06E-04	0.26608
2.87	0.28531	1.76499	4.71E-04	0.25039
3.06	0.31042	1.62606	3.77E-04	0.22903
3.25	0.32688	1.5081	3.04E-04	0.20579
3.45	0.34897	1.39262	2.47E-04	0.17746
3.64	0.3656	1.28907	1.99E-04	0.14746
3.83	0.36952	1.20879	1.57E-04	0.12481
4.03	0.35272	1.15895	1.20E-04	0.11487
4.22	0.33741	1.11147	9.29E-05	0.10186
4.41	0.32559	1.06597	7.13E-05	0.09384
4.61	0.31287	1.02705	5.53E-05	0.08789
4.8	0.30015	0.99207	4.26E-05	0.08666
5	0.26802	0.97857	3.12E-05	0.0922
5.5	0.37823	0.76513	1.93E-05	0.08379

Table S7. Relaxation fitting parameters from the least-square fitting of the Cole-Cole plots of 5 by the single-component generalized Debye model at 1000 Oe dc fields.

T (K)	χ_s (emu/mol)	$\Delta\chi$ (emu/mol)	τ (s)	α
At 1 kOe dc field				
1.9	0.05412	0.61804	1.14E-03	0.1604
2	0.05468	0.57936	1.01E-03	0.14998
2.1	0.05061	0.55568	9.02E-04	0.15357
2.4	0.04091	0.49509	6.65E-04	0.15014
2.6	0.04088	0.45462	5.58E-04	0.13852
2.8	0.03536	0.42639	4.68E-04	0.13627
3	0.03563	0.39597	4.01E-04	0.12501
3.2	0.0308	0.37657	3.40E-04	0.12467
3.4	0.03292	0.35097	2.99E-04	0.10998
3.6	0.02646	0.33692	2.51E-04	0.11149
3.8	0.02867	0.31503	2.21E-04	0.09576
4	0.0268	0.30021	1.88E-04	0.09477
4.2	0.03346	0.27765	1.68E-04	0.07698
4.4	0.02136	0.27628	1.38E-04	0.08242
4.6	0.02122	0.263	1.20E-04	0.07285
4.8	0.02673	0.24608	1.07E-04	0.06072
5	0.02904	0.23255	9.48E-05	0.04531
5.5	0.01971	0.21796	6.40E-05	0.02558
6	0.01 (Fixed)	0.20827	4.30E-05	0.01708

Table S8. The splitting of the lowest multiplets for Ln^{III} ions in **1-6** compounds calculated by CASSCF method

Compound	1	2	3	4	5	6
Ln	Dy	Tb	Ho	Er	Yb	Dy
	0	0	0	0	0	0
	0	0.07	1.16	0	0	0
	160.78	114.26	136.77	57.34	277.26	155.22
	160.78	115.42	153.08	57.34	277.26	155.22
	305.67	201.91	172.74	116.8	460.12	308.09
	305.67	206.96	188.43	116.8	460.12	308.09
	362.81	320.16	220.63	162.67	658.68	366.08
	362.81	330.79	240.28	162.67	658.68	366.08
Energy levels (cm⁻¹)	467.97	421.59	252.46	205.5		461.29
	467.97	483.36	281.23	205.5		461.29
	500	524.71	301.21	262.98		524.81
	500	647.76	322.81	262.98		524.81
	566.61	656.54	353.22	304.43		557.12
	566.61		372.73	304.43		557.12
	639.45		392.21	467.57		631.23
	639.45		431.14	467.57		631.23
			437.27			
Calculated spin-orbit interactions (cm⁻¹)	1928	1732	2142	2372	2880	1928

Table S9. The g-factors for the effective spin 1/2 calculated by CASSCF for lowest Kramers (pseudo)doublets of **1-6**.

complex 1 (Dy ^{III})			
<i>E</i> (cm ⁻¹)	<i>g_x</i>	<i>g_y</i>	<i>g_z</i>
0	0.008730	0.010438	19.785687
161	0.104307	0.129858	17.107310
306	2.678054	6.545777	10.780921
complex 2 (Tb ^{III}) ^a			
<i>E</i> (cm ⁻¹)	<i>g_x</i>	<i>g_y</i>	<i>g_z</i>
0.0360707	0.0	0.0	17.826389
114.8369735	0.0	0.0	15.282851
204.4346824	0.0	0.0	11.747221
complex 3 (Ho ^{III}) ^a			
<i>E</i> (cm ⁻¹)	<i>g_x</i>	<i>g_y</i>	<i>g_z</i>
0.57919	0.0	0.0	18.949454
complex 4 (Er ^{III})			
<i>E</i> (cm ⁻¹)	<i>g_x</i>	<i>g_y</i>	<i>g_z</i>
0	0.886047	2.602348	14.051874
57	3.674964	4.638638	7.799773
117	1.862991	2.756479	8.899551
complex 5 (Yb ^{III})			
<i>E</i> (cm ⁻¹)	<i>g_x</i>	<i>g_y</i>	<i>g_z</i>
0	0.933863	2.183350	6.616699
277	1.377984	2.853956	3.243385
460	0.424653	1.025765	5.951962
complex 6 (Dy ^{III})			
<i>E</i> (cm ⁻¹)	<i>g_x</i>	<i>g_y</i>	<i>g_z</i>
0	0.007161	0.007706	19.789033
155	0.100681	0.118645	17.095825
308	2.517330	5.002615	11.919597

^a energy values correspond to the average values of two respective levels.

Table S10. Comparison of U_{eff} value of this work with the other reported mononuclear Yb^{III} SMMs.^a

Compound	Field (Oe)	$U_{\text{eff}}(\text{K})$	$\tau_0(\text{s})$	Ref.
Yb(trensal)	2000	54.7	1.5×10^{-8}	S1
[Yb(L ³) ₂ (TMH)(CH ₃ OH)]	1000	29.7	3.5×10^{-7}	S2
[Yb(tta)(CH ₃ OH)]	1000	30.3	2.0×10^{-7}	S2
[Yb(H ₃ Bmshp)(DMF) ₂ Cl ₂].H ₄ Bmshp	600	38.3	7.16×10^{-7}	S3
[Yb(PyrCOO)(acac) ₂ (H ₂ O) ₂]	1000	54	7.4×10^{-8}	S4
[Ln(NAS) ₂ (H ₂ O) ₆](NAS).3H ₂ O	1000	45	5.1×10^{-8}	S5
[Yb(depma) ₂ (H ₂ O) ₆]Cl ₂ .3H ₂ OCH ₃ O	750	28.9	4.6×10^{-8}	S6
[Yb(H ₂ O) ₆ (NCS) ₃].H ₂ O	2500	50	2.3×10^{-8}	S7
[Yb(H ₂ O) ₆ (bpy) ₂ (NCS) ₃].0.5(bpy).H ₂ O	1000	47	1.7×10^{-8}	S7
[Hbpy][Yb(bpy) ₂ (NCS)4].H ₂ O	1000	44	2.9×10^{-8}	S7
[Hphen][Yb(phen) ₂ (NCS)4]	1000	37	8.4×10^{-8}	S7
[Yb(Ph ₃ PO) ₄ (OTf) ₂][OTf]	2000	28.2 (SR)	2.88×10^{-8}	S8
	2000	27.0 (FR)	3.0×10^{-7}	
5	1000	39	1.4×10^{-7}	This work

^a U_{eff} values 25 K onwards are assembled in the table; trensal = 2,2',2''-tris(salicylideneimino)triethylamine; HL³ = 2-(tetrazol-5-yl)-1,10-phenanthroline; TMH = 2,2,6,6-tetramethylheptanoate; tta = 2-thenoyltrifluoroacetone; H₄Bmshp = (2,6-bis[(3-methoxysalicylidene)hydrazinecarbonyl]-pyridine); PyrCOOH = pyrazine-2-carboxylic acid; acac = acetylacetone; NAS = 2-naphthalenesulfonate; depma = 9-diethylphosphono-methylanthracene; bpy = 2,2'-bipyridine; phen = 1,10-phenanthroline; Ph₃PO = Triphenylphosphine oxide; OTf = Trifluoromethanesulfonate.

Table S11. Comparison of U_{eff} value of this work with the other reported Dy^{III} SMMs with N-salicylideneaniline type ligands in the zwitterionic form.^a

Compound	Field (Oe)	$U_{\text{eff}}(\text{K})$	$\tau_0(\text{s})$	Ref.
[Dy(HL ⁴) ₂ (NO ₃) ₃]	2000	22.8	4.2×10^{-7}	39
[Dy(HL ⁴) ₂ (NO ₃) ₃]	2000	22.7	2.47×10^{-6}	40
		22.5	3.6×10^{-7}	
[Dy(NO ₃) ₃ (5BrsalanH) ₂ (H ₂ O)]·MeCN	1000	38.5	2.5×10^{-6}	41
[Dy(NO ₃) ₃ (salanH) ₂ (H ₂ O)]·MeCN	1000	18.7	4.5×10^{-7}	42
[Dy(NO ₃) ₃ (salanH) ₂ (MeOH)]·(salanH)	1000	44.3	2.5×10^{-7}	42
[Dy(HL ⁵) ₂ (NO ₃) ₃ (CH ₃ OH)]	0	62	1.0×10^{-7}	43
	1000	66.6	9.0×10^{-8}	
[Dy(HL ⁶) ₂ (NO ₃) ₃ (CH ₃ OH)]	1000	67	9.72×10^{-8}	44
[Dy(HL ⁷) ₂ (NO ₃) ₃ (H ₂ O)]	0	43	1.2×10^{-7}	44
	1000	116	8.72×10^{-11}	
[Dy(HL ⁸) ₃ (NO ₃) ₃]·CH ₃ CN	1000	66	1.29×10^{-7}	44
[Dy(HL ⁹) ₃ (NO ₃) ₃]	1000	62	6.11×10^{-10}	44
1	0	20.7	$6.7 \cdot 10^{-9}$	This work
	1000	52.8	$7.6 \cdot 10^{-9}$	
6	0	151	$2.0 \cdot 10^{-8}$	This work
	1000	221	$1.9 \cdot 10^{-9}$	

^a HL³ = 2-methoxy-6-[(E)-phenyliminomethyl]phenol; 5BrsalanH = *N*-(5-bromosalicylidene)aniline; salanH = 2-(phenyliminomethyl)phenol; HL⁴ = 1-[*N*-(4-bromophenyl)]aminomethylidene]-2(1*H*)naphthalenone; HL⁵ = 1-[*N*-(4-chlorophenyl)]aminomethylidene-2(1*H*)naphthalenone; HL⁶ = (1-[*N*-(4-nitrophenyl)]aminomethylidene)-2(1*H*)-naphthalenone; HL⁷ = (1-[*N*-(4-methoxyphenyl)]aminomethylidene)-2(1*H*)-naphthalenone; HL⁸ = (1-[*N*-(4-iodophenyl)]aminomethylidene)-2(1*H*)-naphthalenone;

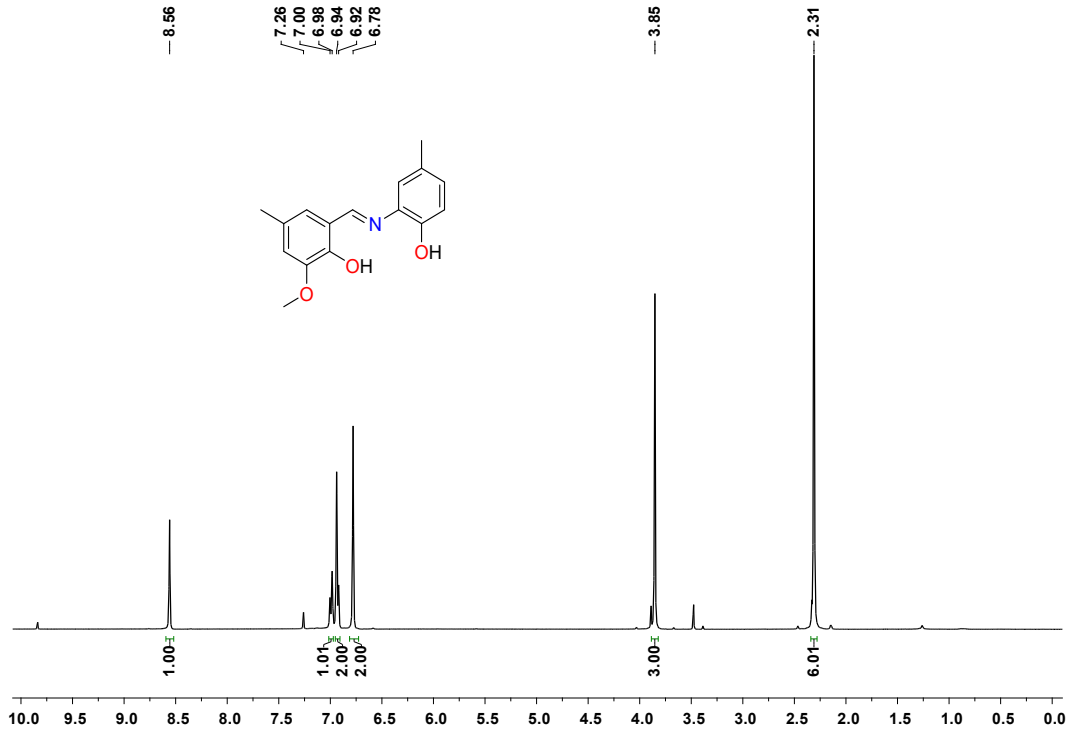


Fig. S1. ¹H NMR spectrum of ligand LH in CDCl_3 at r.t.

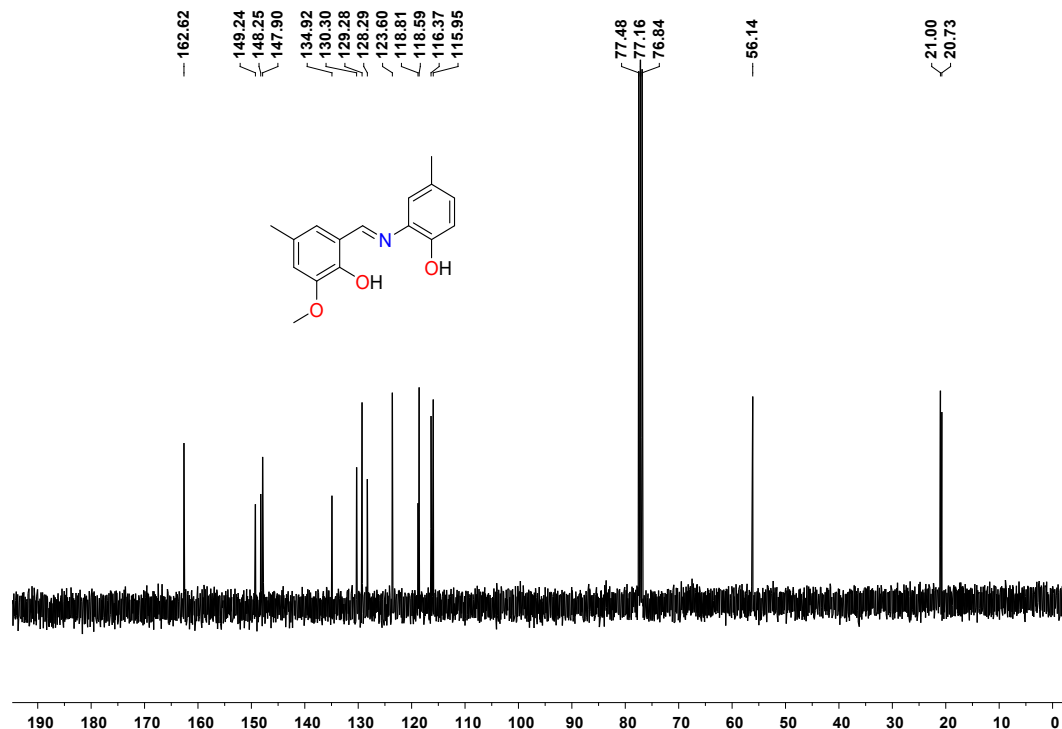


Fig. S2. ¹³C NMR of ligand LH in CDCl_3 at r.t.

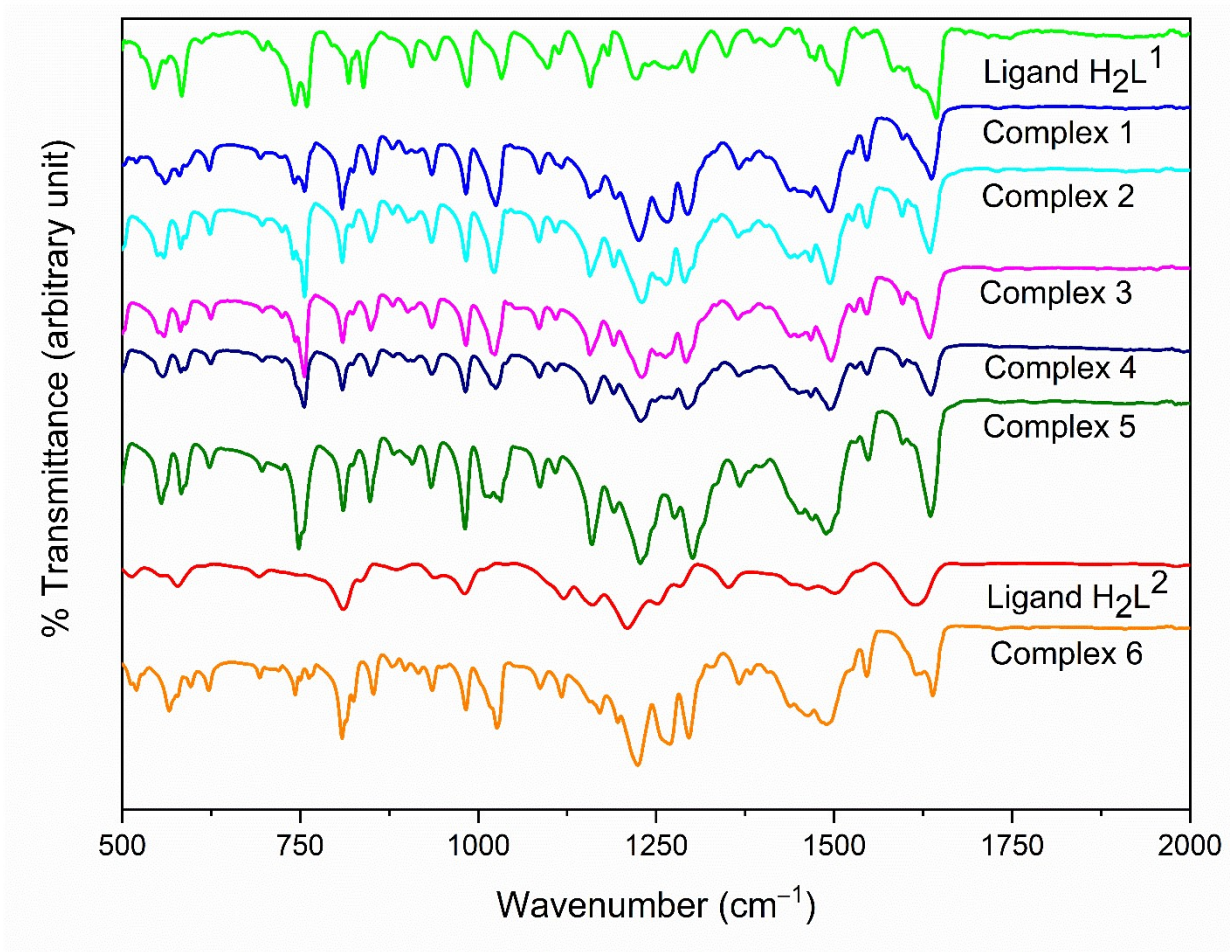


Fig. S3. IR spectra of the ligands and complexes **1-6**.

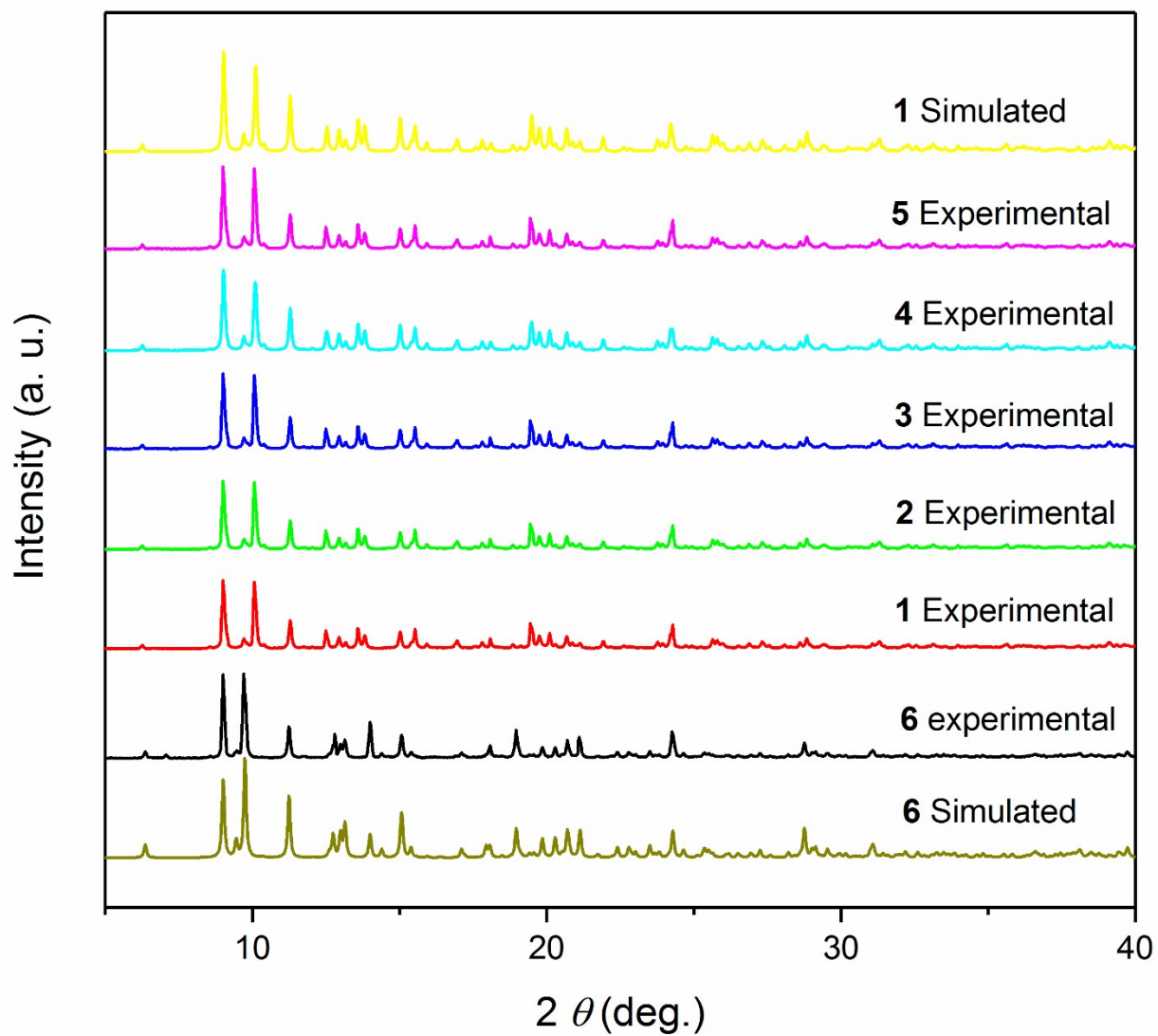


Fig. S4. Experimental and simulated PXRD patterns of complexes 1-6.

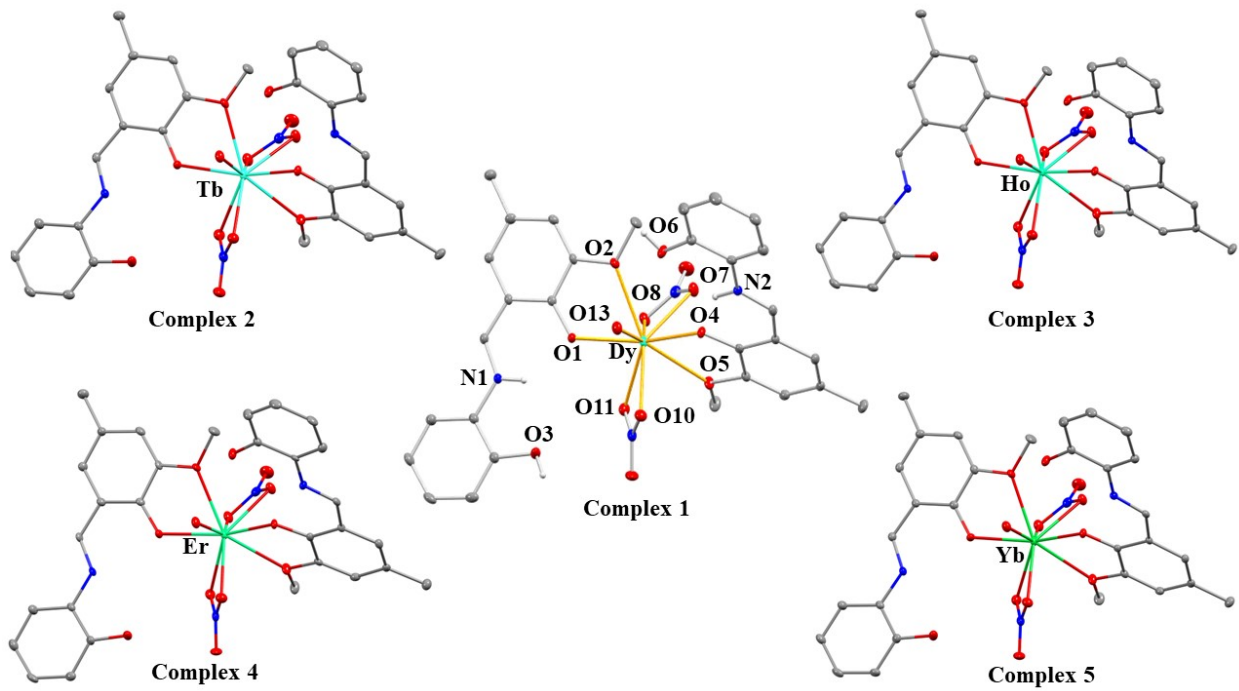


Fig. S5. Crystal structures of complexes 1-5 with ellipsoid plots (probability level 30 %)

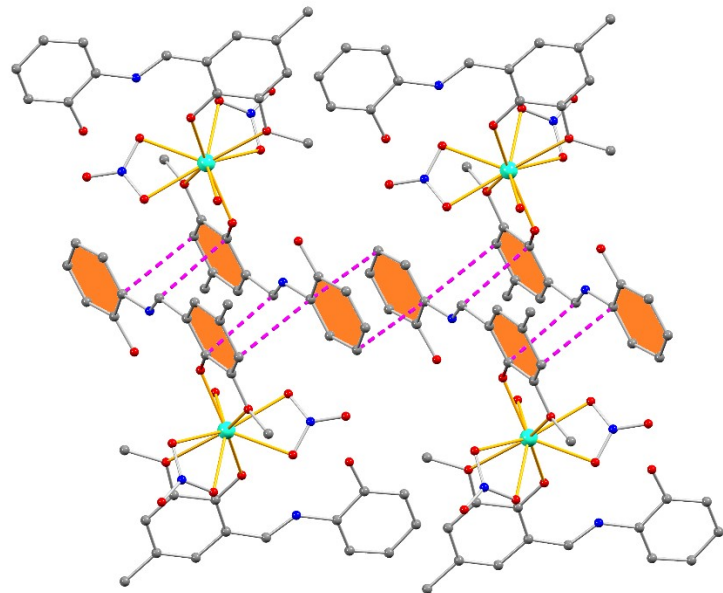


Fig. S6: Crystal packing of complex 1 focusing on the $\pi\cdots\pi$ stacking interaction

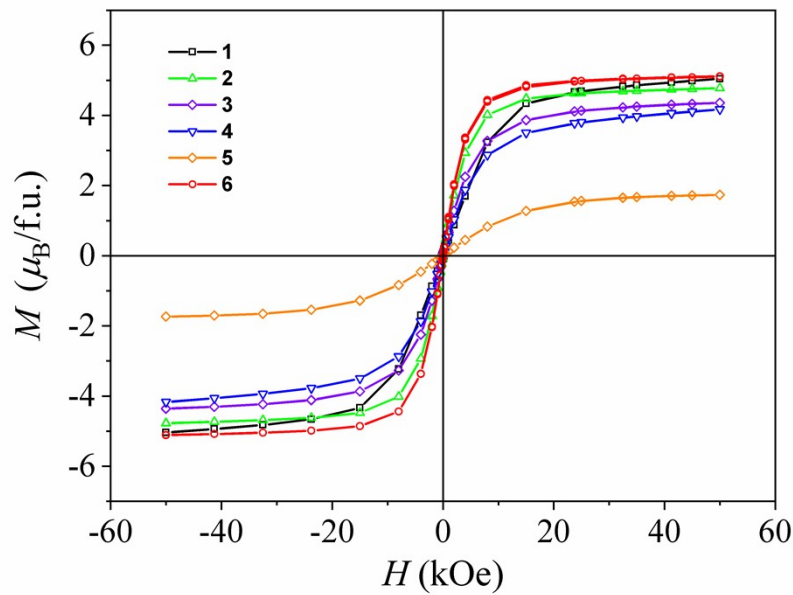


Fig. S7. Isothermal magnetization curves for complexes **1-6** at 2 K.

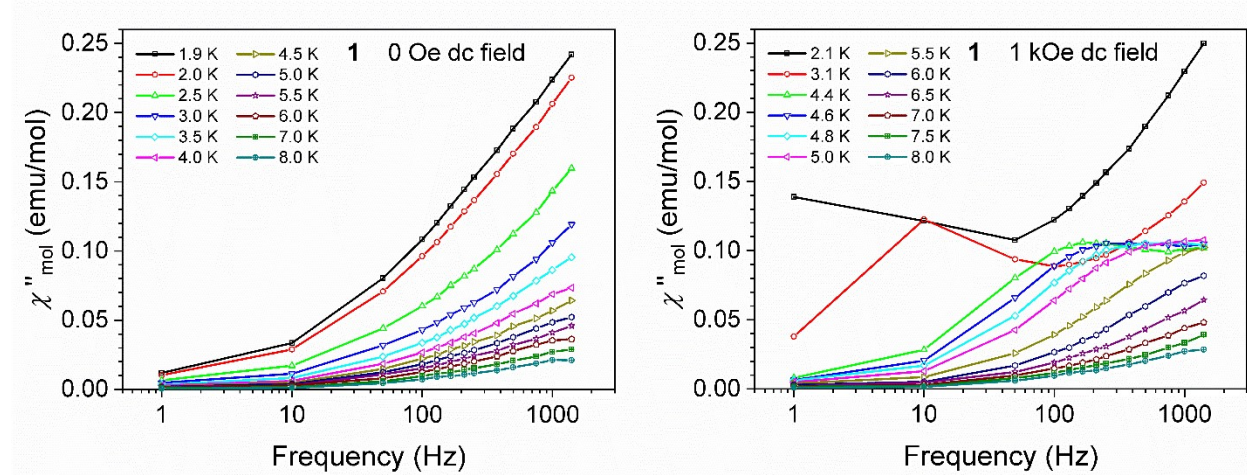


Fig. S8. Frequency dependent out-of-phase ac susceptibility plots of **1** in zero dc field (left) and 1 kOe dc field (right).

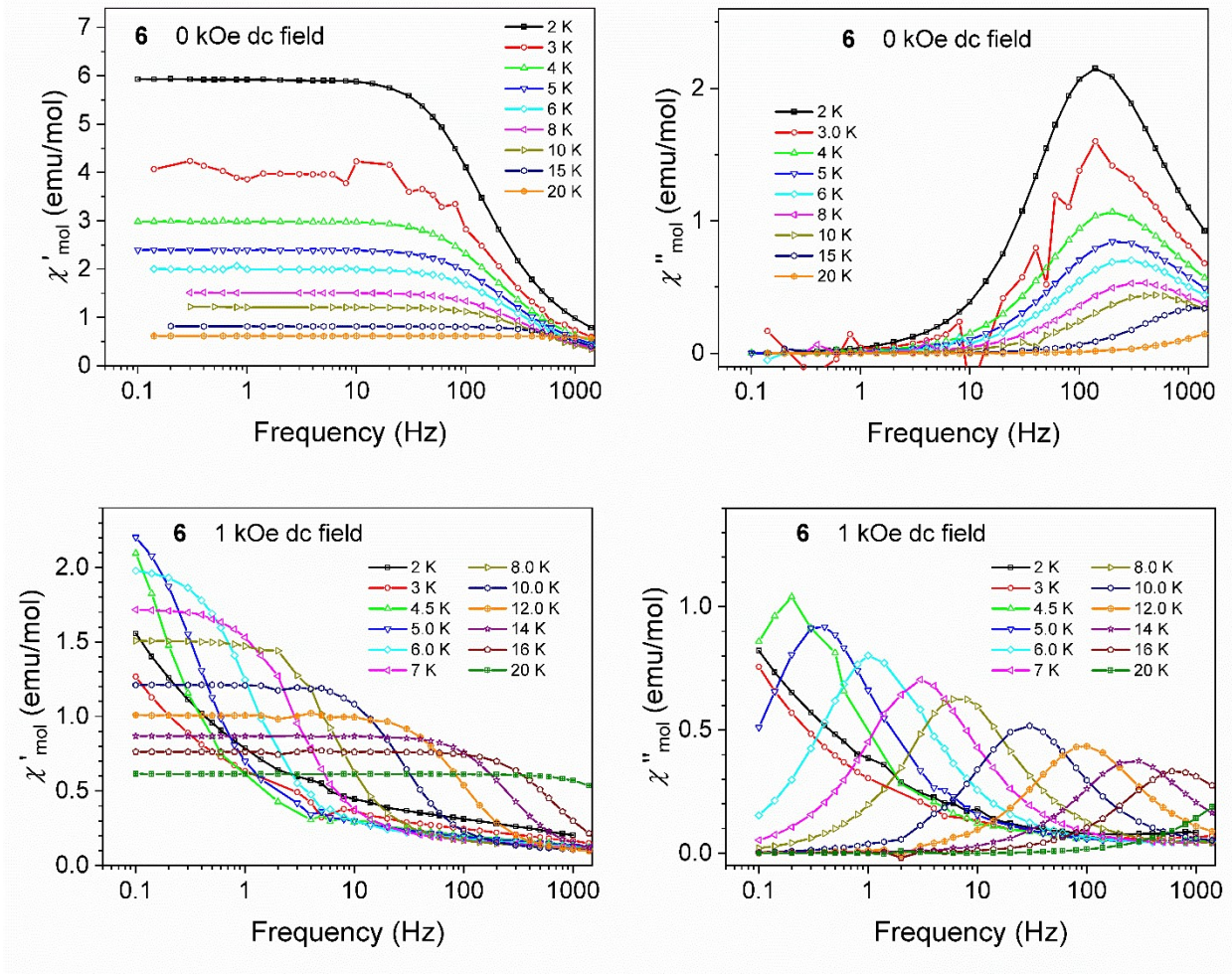


Fig. S9. Frequency dependent in-phase and out-of-phase ac susceptibility plots of **6** at indicated dc field.

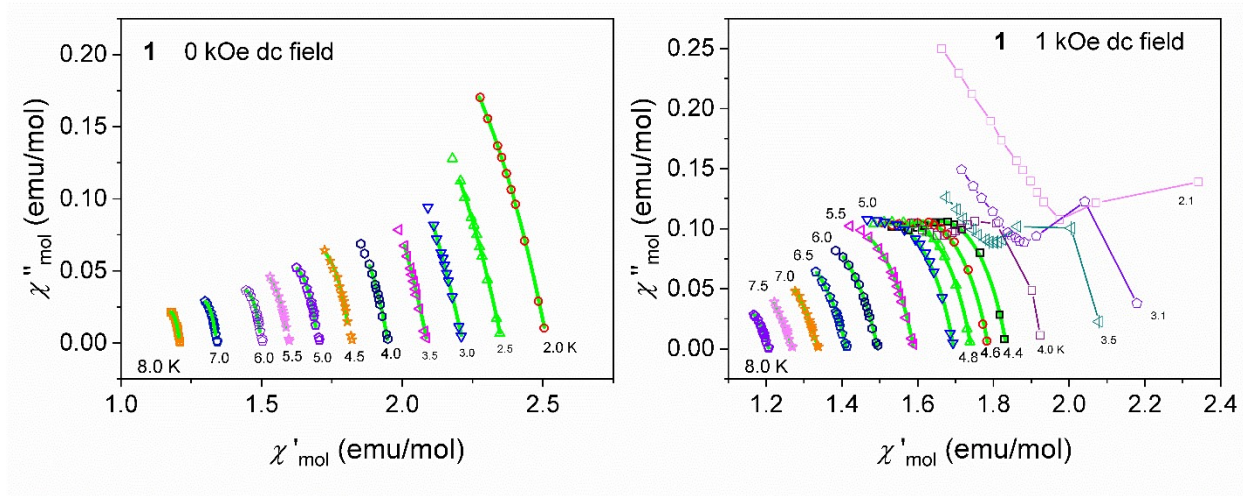


Fig. S10. Cole-Cole plot for **1** at zero dc field (left) and 1 kOe dc field (right)

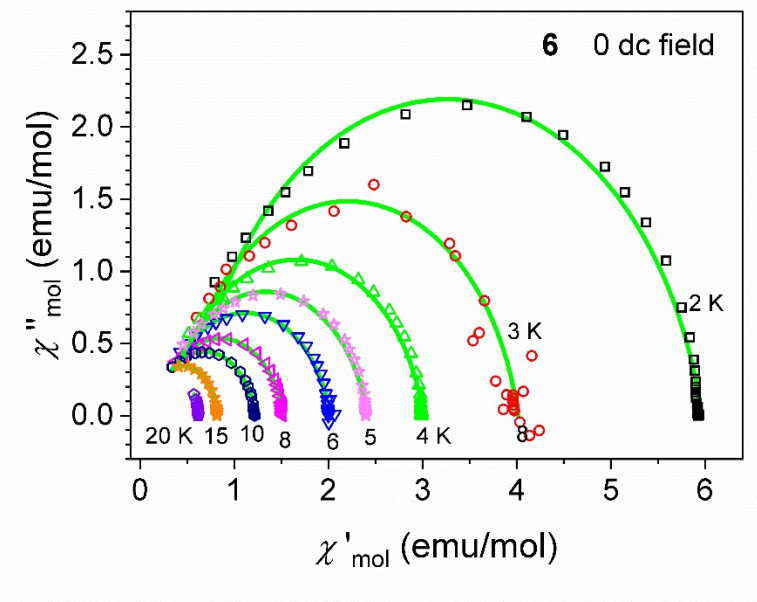


Fig. S11. Cole-Cole plot for **6** at zero dc field.

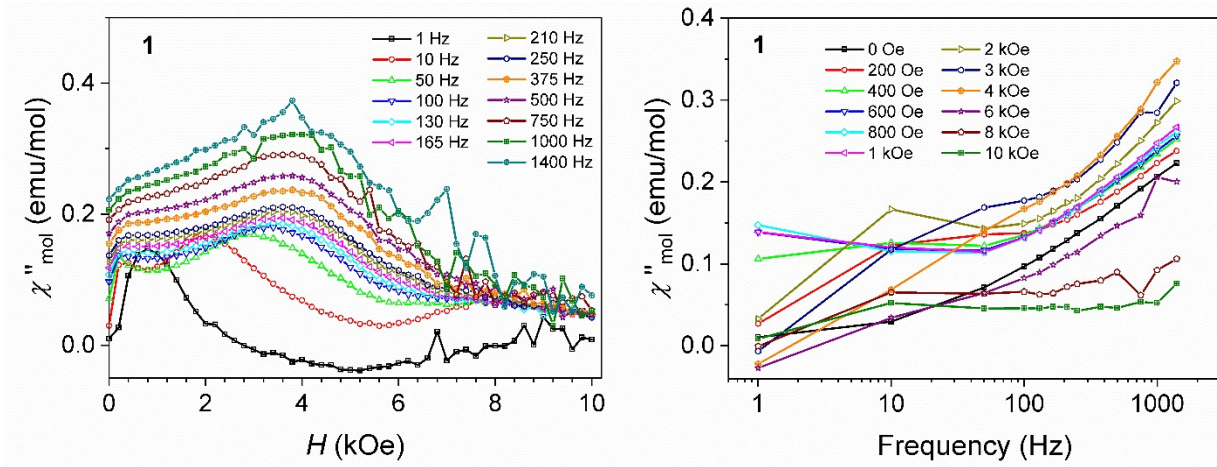


Fig. S12. Out-of-phase ac susceptibility as a function of dc magnetic field (left) and frequency (right) for 1 measured at 2 K.

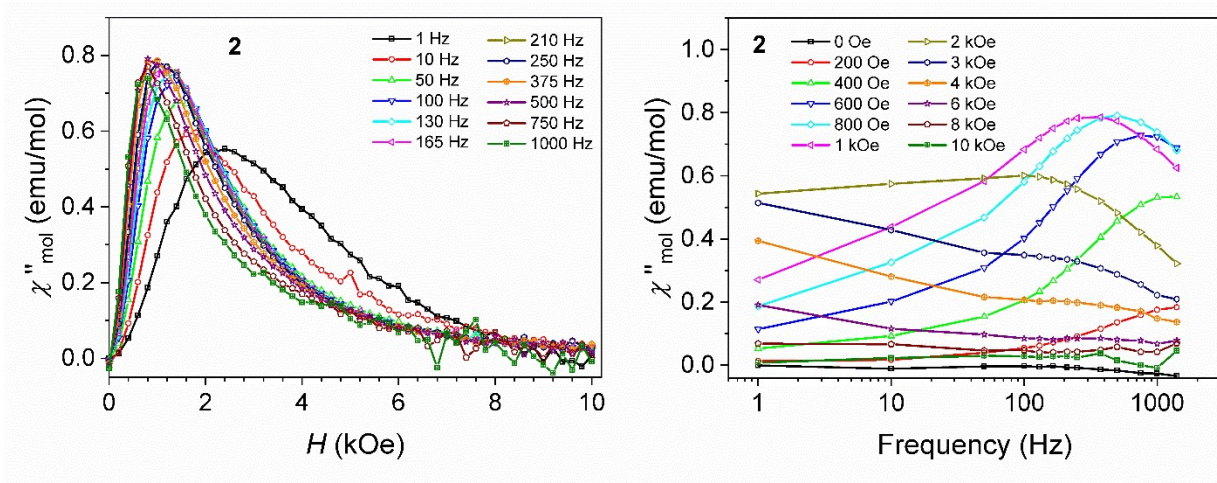


Fig. S13. Out-of-phase ac susceptibility as a function of dc magnetic field (left) and frequency (right) for 2 measured at 2 K.

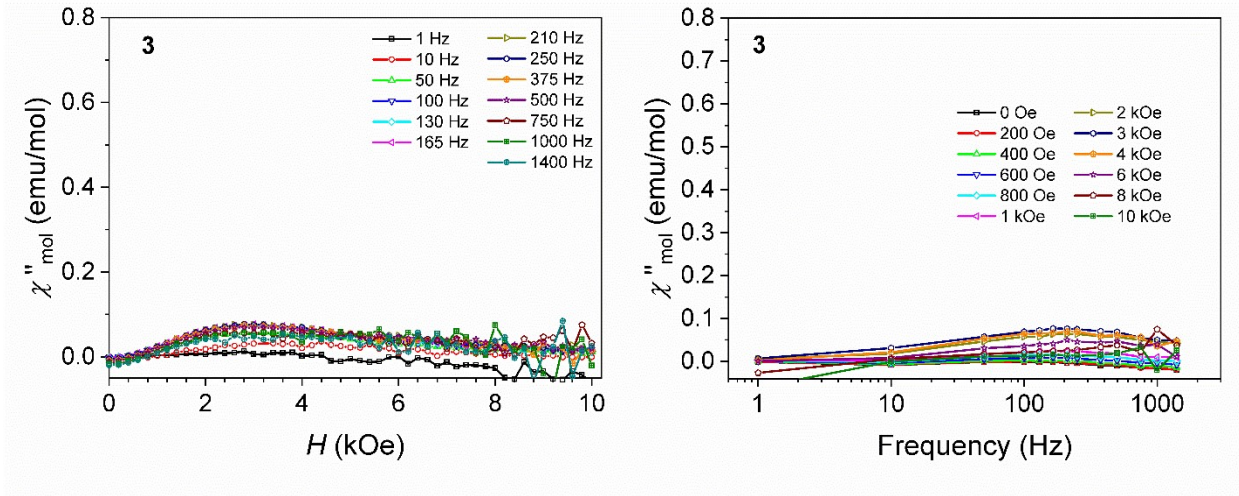


Fig. S14. Out-of-phase ac susceptibility as a function of dc magnetic field (left) and frequency (right) for 3 measured at 2 K.

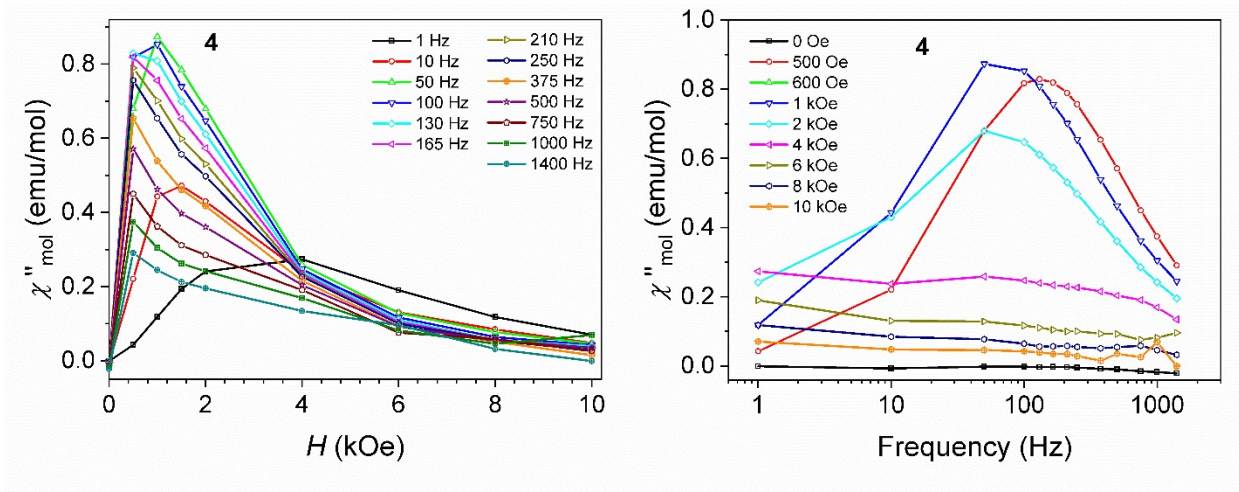


Fig. S15. Out-of-phase ac susceptibility as a function of dc magnetic field (left) and frequency (right) for 4 measured at 1.9 K.

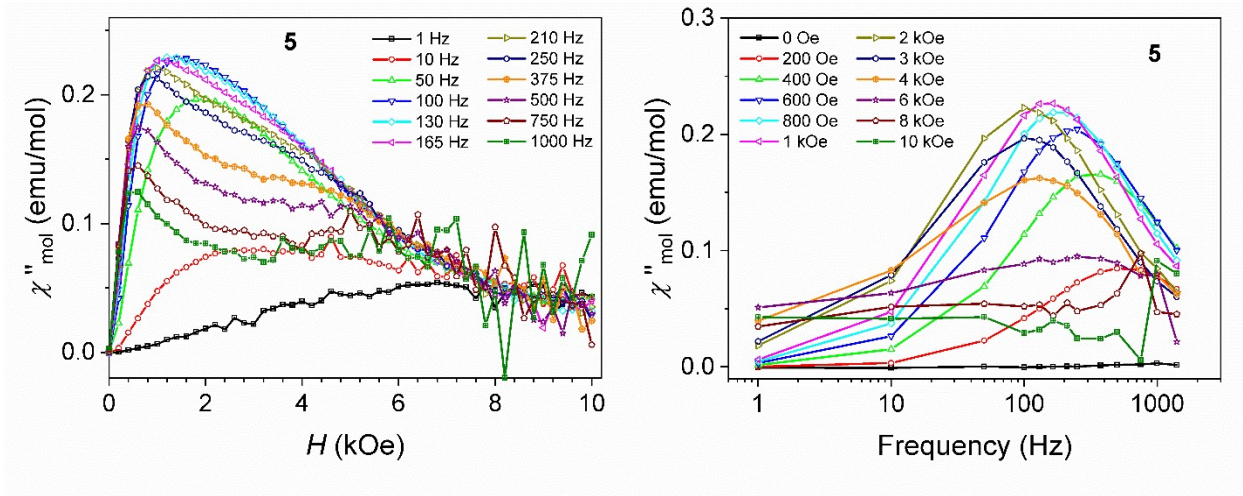


Fig. S16. Out-of-phase ac susceptibility as a function of dc magnetic field (left) and frequency (right) for **5** measured at 2 K.

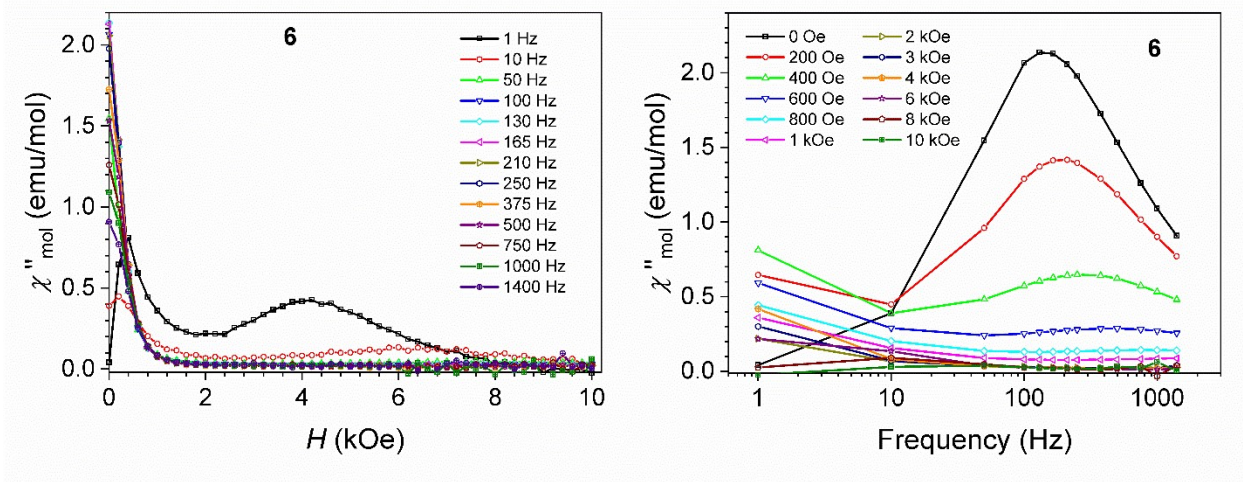


Fig. S17. Out-of-phase ac susceptibility as a function of dc magnetic field (left) and frequency (right) for **6** measured at 2 K.

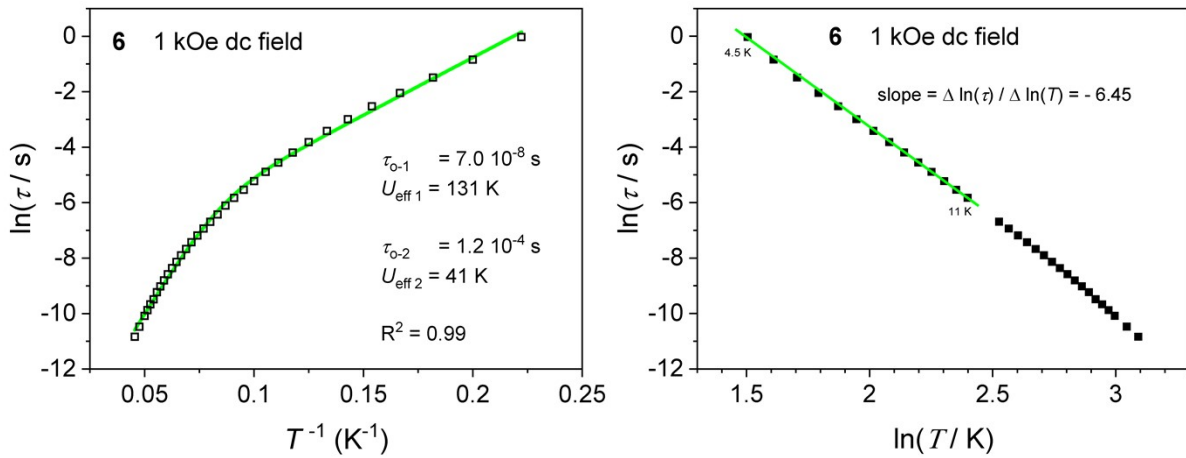


Fig. S18. The plot of magnetisation relaxation time in the form of $\ln(\tau)$ vs. T^{-1} (left) and $\ln(\tau)$ vs. $\ln(T)$ (right); solid lines in the plots denoting the best fit considering only two Orbach like relaxations (left) and the linear fit (right); insets showing the best fit parameters.

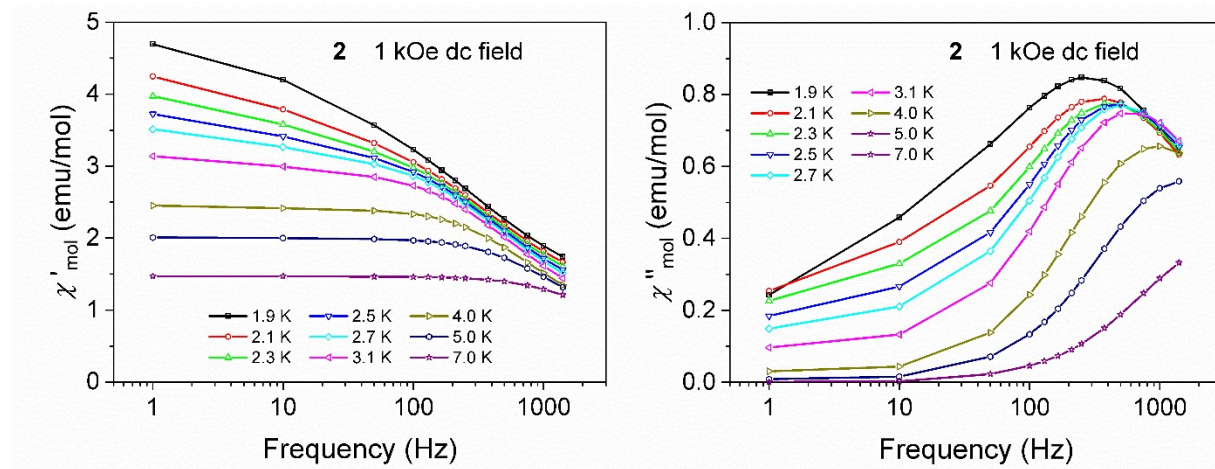


Fig. S19. Frequency dependent in-phase and out-of-phase ac susceptibility plots of **2** at indicated dc field.

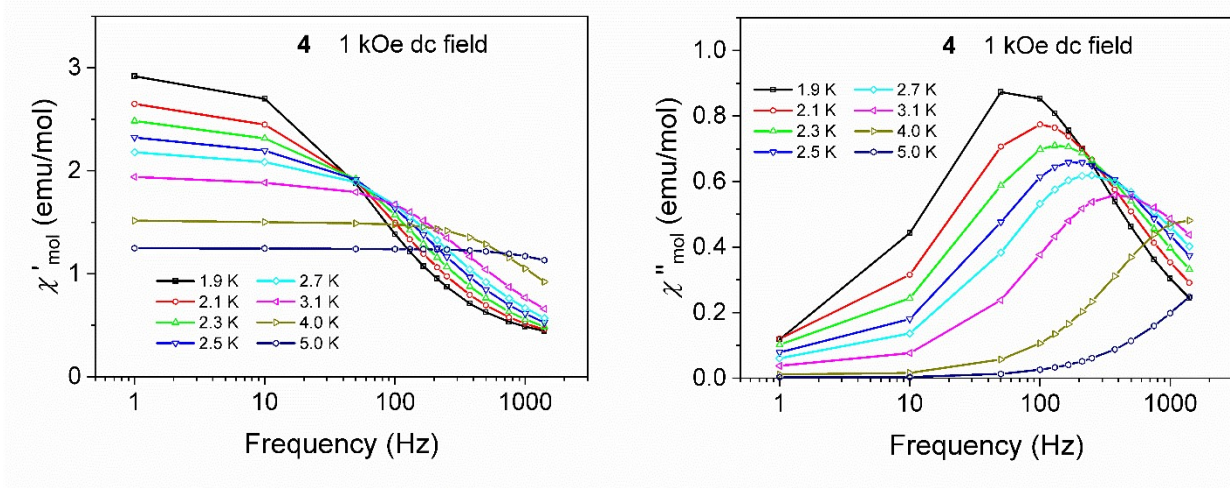


Fig. S20. Frequency dependent in-phase and out-of-phase ac susceptibility plots of **4** at indicated dc field.

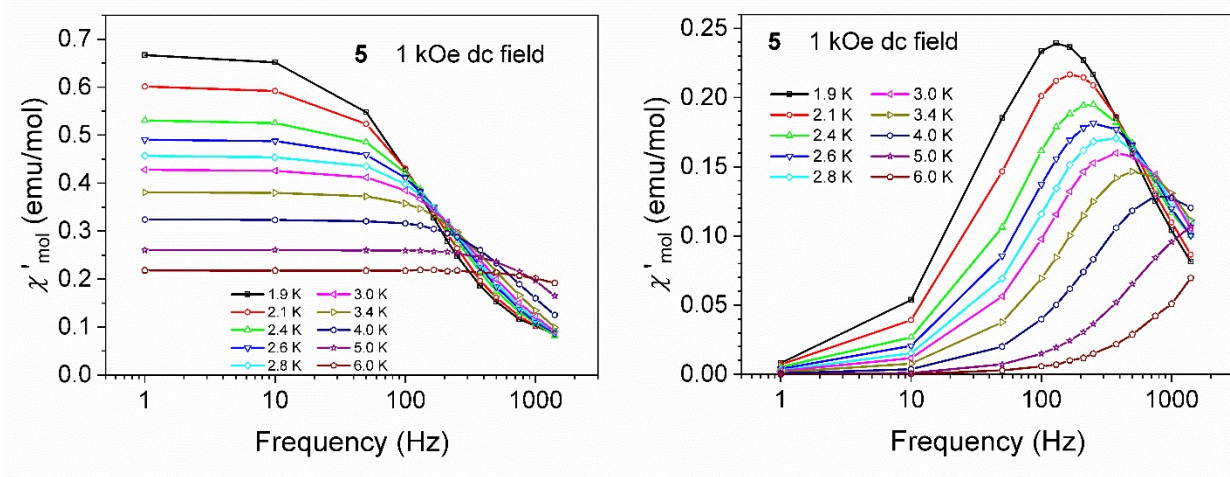


Fig. S21. Frequency dependent in-phase and out-of-phase ac susceptibility plots of **5** at indicated dc field.

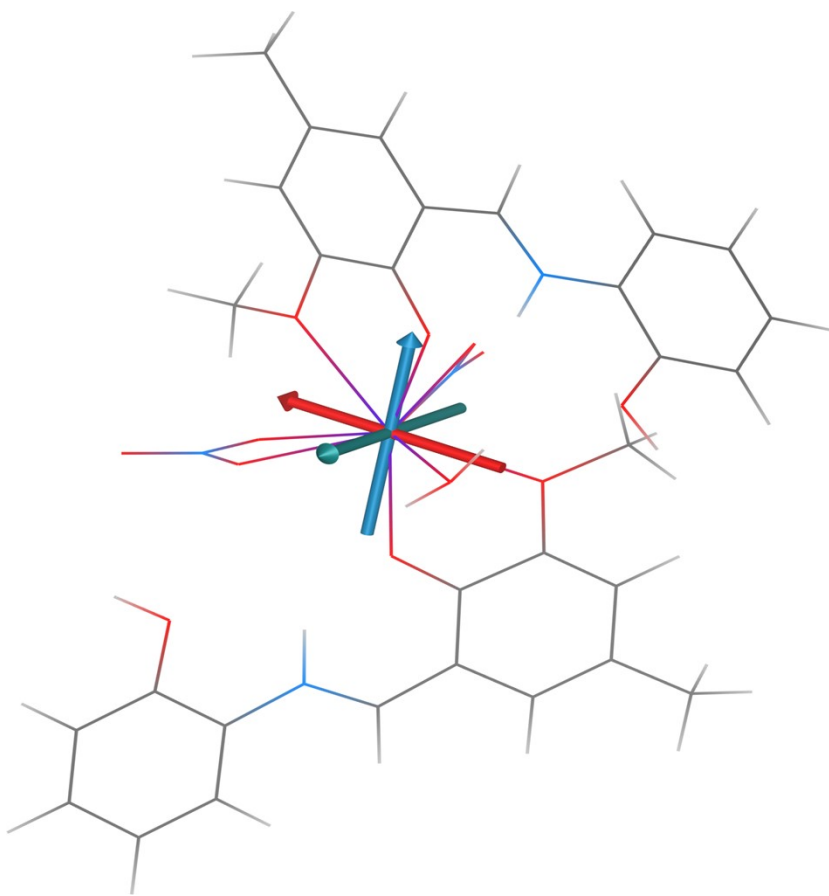


Fig. S22 The molecular structure of complex **1** derived from the experimental X-ray geometry used for CASSCF calculations done in ORCA overlaid with principal axis of g-tensor of the first Kramers doublet (x/y/z-axes colored as red/green/blue arrows).

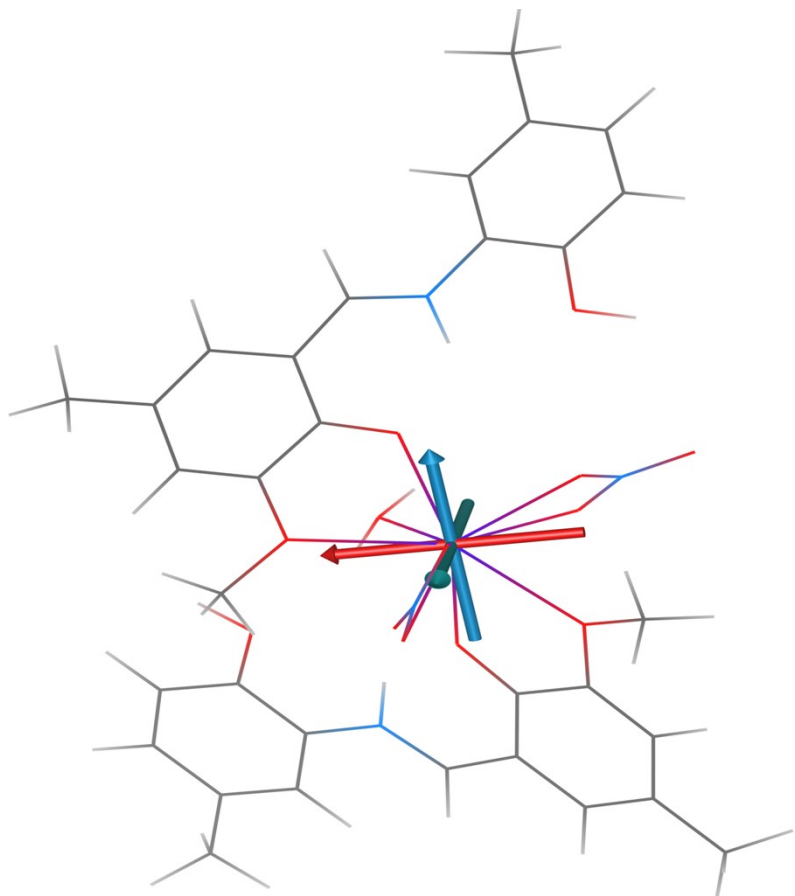


Fig. S23 The molecular structure of complex **6** derived from the experimental X-ray geometry used for CASSCF calculations done in ORCA overlaid with principal axis of g-tensor of the first Kramers doublet (x/y/z-axes colored as red/green/blue arrows).

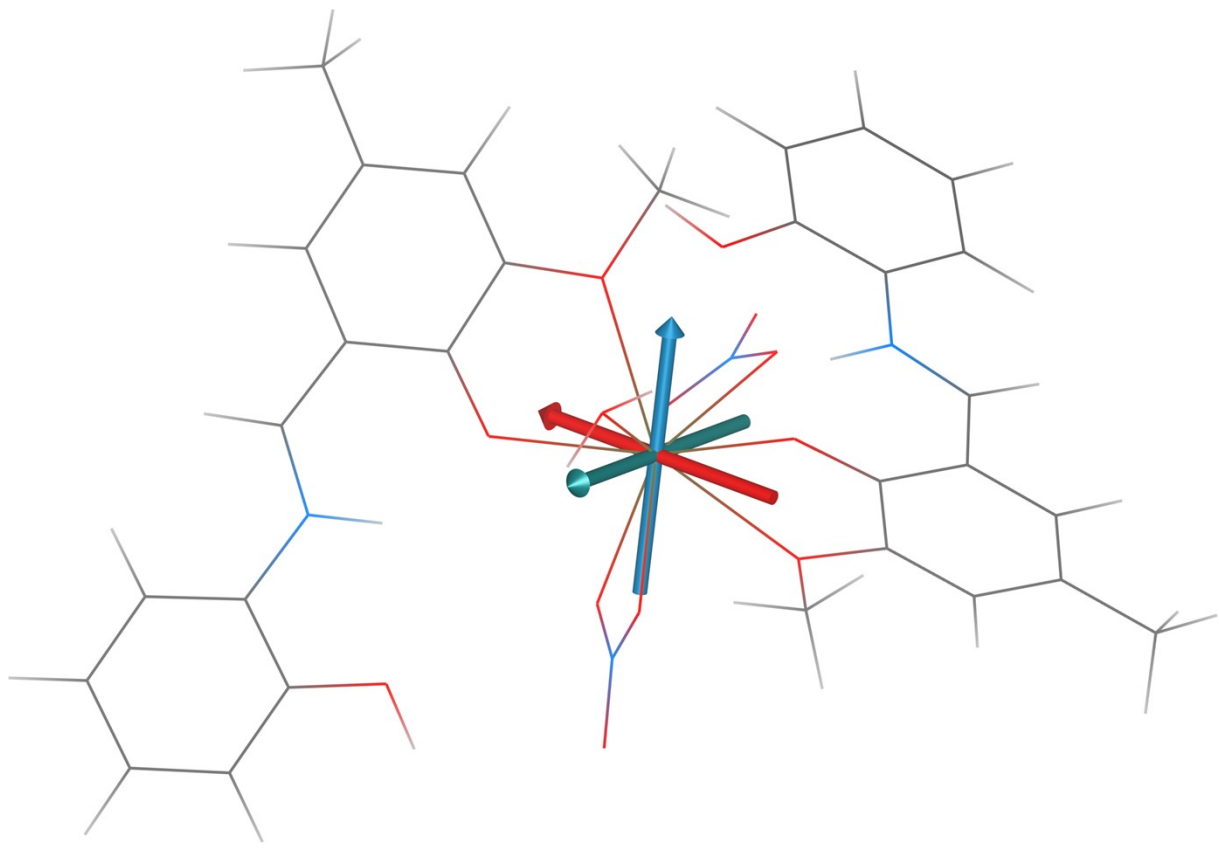


Fig. S24 The molecular structure of complex 4 derived from the experimental X-ray geometry used for CASSCF calculations done in ORCA overlaid with principal axis of g-tensor of the first Kramers doublet (x/y/z-axes colored as red/green/blue arrows).

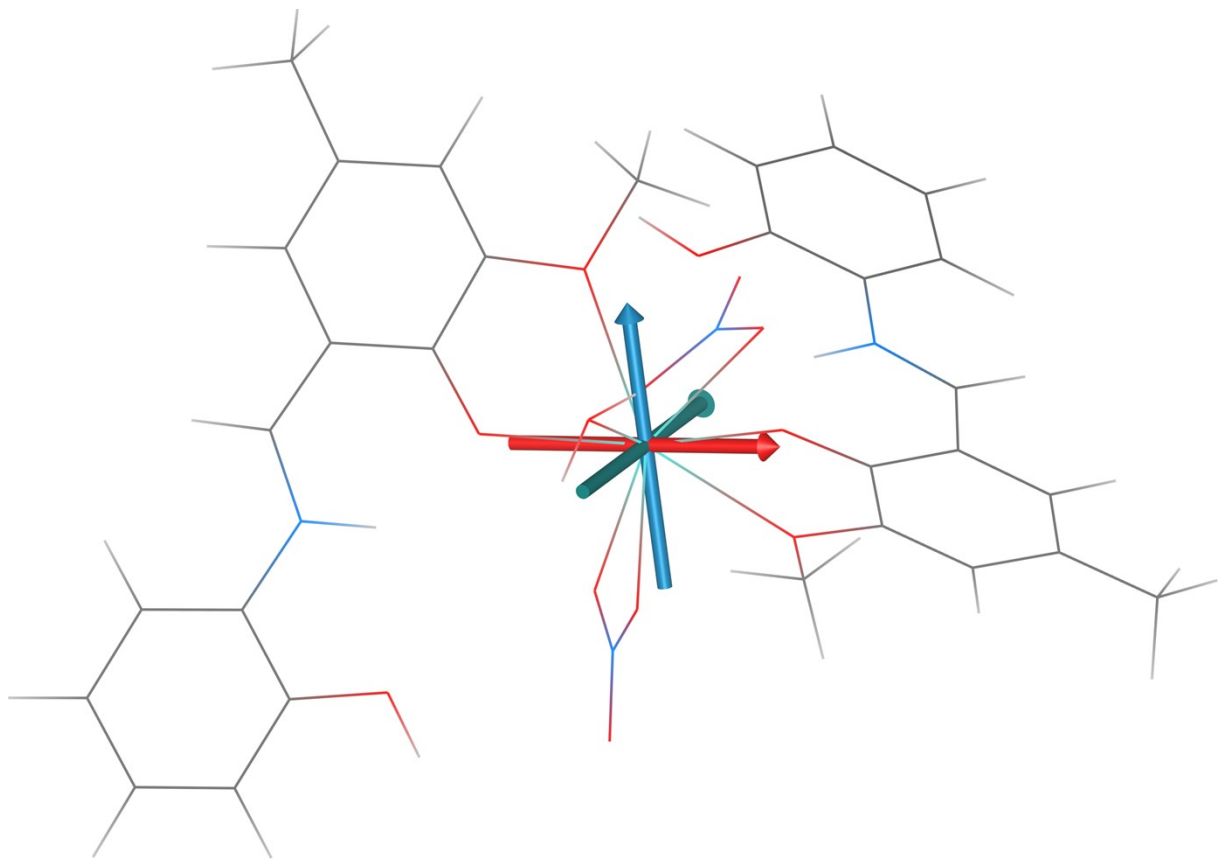


Fig. S25 The molecular structure of complex **5** derived from the experimental X-ray geometry used for CASSCF calculations done in ORCA overlaid with principal axis of g-tensor of the first Kramers doublet (x/y/z-axes colored as red/green/blue arrows).

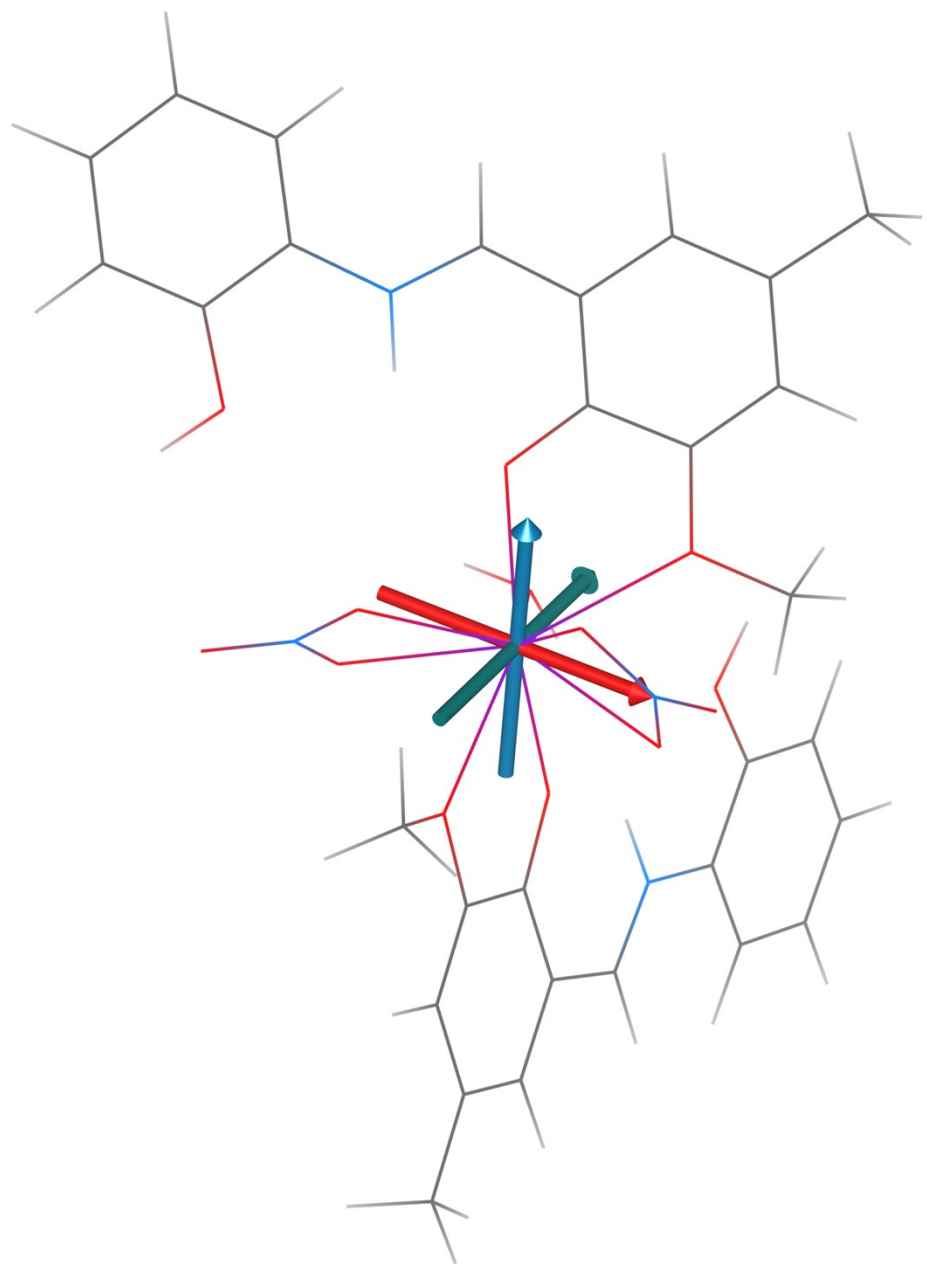


Fig. S26 The molecular structure of complex **2** derived from the experimental X-ray geometry used for CASSCF calculations done in ORCA overlaid with principal axis of g-tensor of the first Kramers doublet (x/y/z-axes colored as red/green/blue arrows).

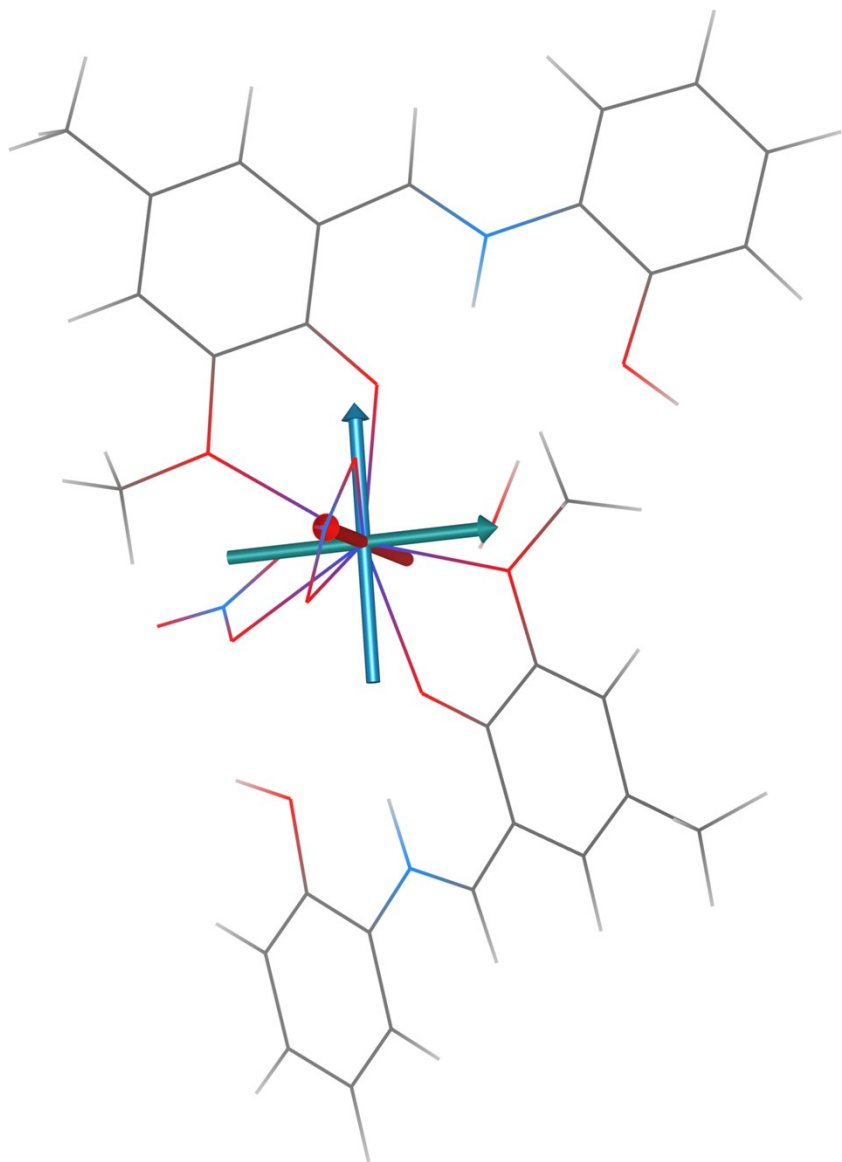


Fig. S27 The molecular structure of complex **3** derived from the experimental X-ray geometry used for CASSCF calculations done in ORCA overlaid with principal axis of g-tensor of the first Kramers doublet (x/y/z-axes colored as red/green/blue arrows).

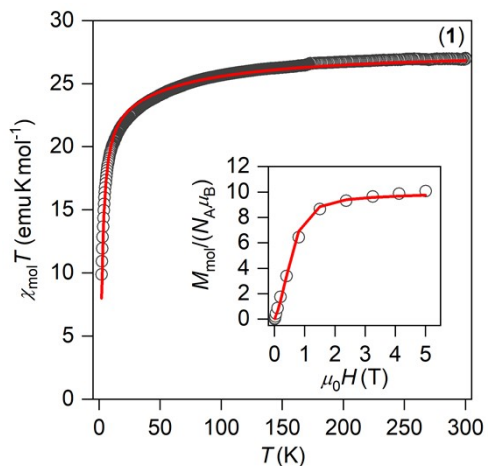
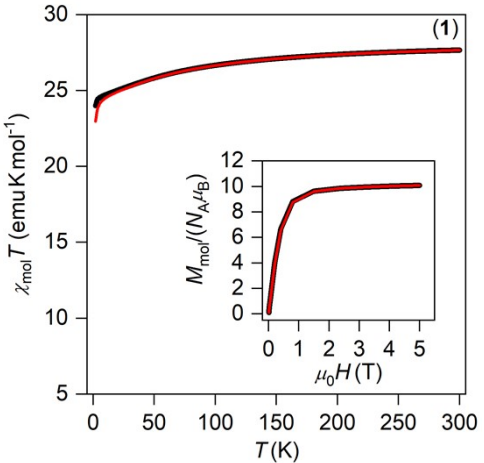
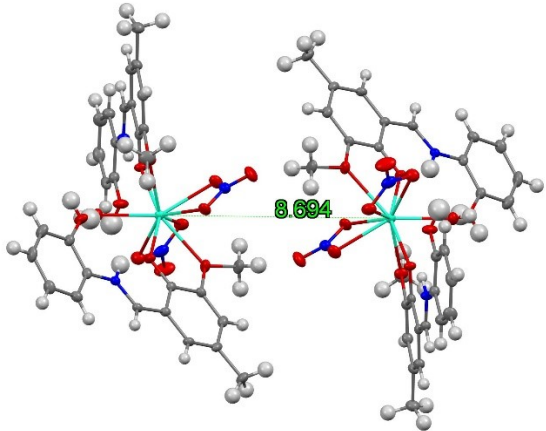
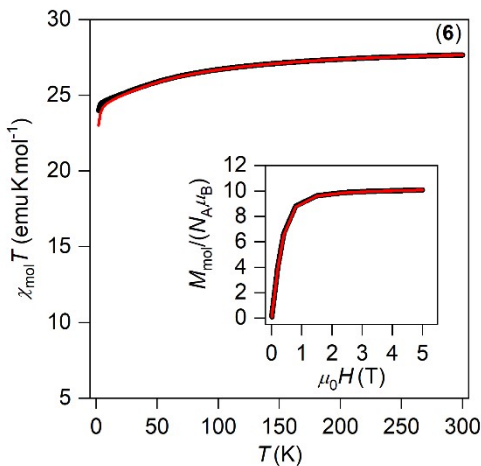
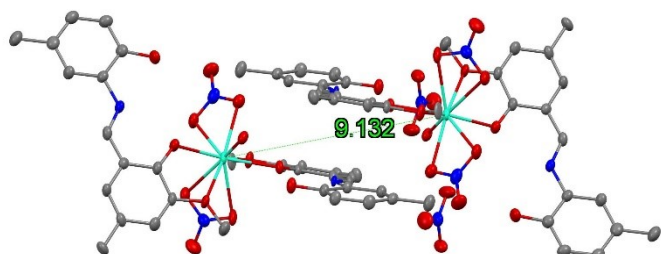


Fig. S28 The analysis of magnetic properties of 1 by POLY_ANISO module. Top: The molecular structure of supramolecular dimer of 1 derived from the experimental X-ray geometry and calculated magnetic data for such dimer using POLY_ANISO program based on respective CASSCF calculations without dipolar interaction (black line) / with dipolar interaction (red line). Bottom: The fit of experimental magnetic data utilizing CASSCF calculations, POLY_ANISO program and homemade routine with the exchange parameter JDy-Dy = -0.180 cm⁻¹, scaling factor for calculated data: 0.973.



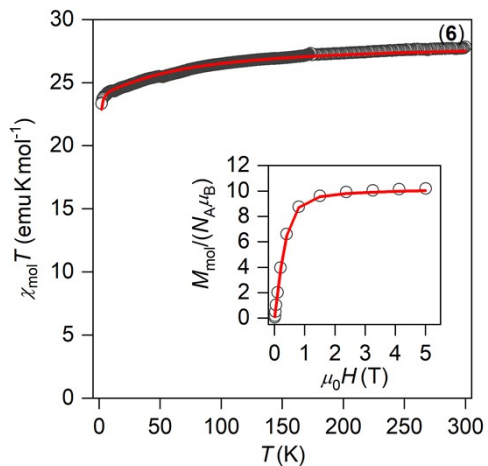


Fig. S29 The analysis of magnetic properties of 6 by POLY_ANISO module. *Top*: The molecular structure of supramolecular dimer of 6 derived from the experimental X-ray geometry and calculated magnetic data for such dimer using POLY_ANISO program based on respective CASSCF calculations without dipolar interaction (black line) / with dipolar interaction (red line). *Bottom*: The fit of experimental magnetic data utilizing CASSCF calculations, POLY_ANISO program and homemade routine with the exchange parameter $J_{\text{Dy-Dy}} = -0.0024 \text{ cm}^{-1}$, scaling factor for calculated data: 0.994.

References:

- S1 K. S. Pedersen, J. Dreiser, H. Weihe, R. Sibille, H. V. Johannesen, M. A. Sørensen, B. E. Nielsen, M. Sigrist, H. Mutka, S. Rols, J. Bendix and S. Piligkos, *Inorg. Chem.*, 2015, **54**, 7600–7606.
- S2 J. R. Jimenez, I. F. Diaz-Ortega, E. Ruiz, D. Aravena, S. J. A. Pope, E. Colacio and J. M. Herrera, *Chem. – Eur. J.*, 2016, **22**, 14548–14559.
- S3 D.-Q. Wu, D. Shao, X.-Q. Wei, F.-X. Shen, L. Shi, Y.-Q. Zhang and X.-Y. Wang, *Dalton Trans.*, 2017, **46**, 12884–12892.
- S4 A. V. Gavrikov, N. N. Efimov, Z. V. Dobrokhotova, A. B. Ilyukhin, P. N. Vasilyev and V. M. Novotortsev, *Dalton Trans.*, 2017, **46**, 11806–11816.

- S5 G. Peng, Y. Y. Zhang, B. Li, X. F. Sun, H. L. Cai, D. J. Li, Z. G. Gu and G. E. Kostakis, *Dalton Trans.*, 2018, **47**, 17349–17356.
- S6 Q. Zou, X.-D. Huang, J.-C. Liu, S.-S. Bao and L.-M. Zheng, *Dalton Trans.*, 2019, **48**, 2735–2740.
- S7 S. P. Petrosyants, K. A. Babeshkin, A. V. Gavrikov, A. B. Ilyukhin, E. V. Belova and N. N. Efimov, *Dalton Trans.*, 2019, **48**, 12644–12655.
- S8 A. Borah, S. Dey, S. K. Gupta, M. G. Walawalkar, G. Rajaraman and R. Murugavel, *Chem. Commun.*, 2020, **56**, 11879–11882.